energies

MDPI

Article

Effect of Mineral Grain and Hydrate Layered Distribution Characteristics on the Mechanical Properties of Hydrate-Bearing Sediments

Zhenhua Han [1,2], Luqing Zhang [1,2,*], Jian Zhou [3], Zhejun Pan [4], Song Wang [1,2] and Ruirui Li [1,2]

[1] Key Laboratory of Shale Gas and Geoengineering, Institute of Geology and Geophysics, Chinese Academy of Sciences, Beijing 100029, China; hanzhenhua@mail.iggcas.ac.cn (Z.H.); wangsong@mail.iggcas.ac.cn (S.W.); rruili1@163.com (R.L.)
[2] Innovation Academy for Earth Science, Chinese Academy of Sciences, Beijing 100029, China
[3] Key Laboratory of Urban Security and Disaster Engineering of Ministry of Education, Beijing University of Technology, Beijing 100021, China; zhoujian@bjut.edu.cn
[4] Key Laboratory of Continental Shale Hydrocarbon Accumulation and Efficient Development, Ministry of Education, Northeast Petroleum University, Daqing 163318, China; zhejun.pan@nepu.edu.cn
* Correspondence: zhangluqing@mail.iggcas.ac.cn; Tel.: +86-10-8299-8644

Abstract: The mechanical characteristics of gas hydrate-bearing sediments (HBS) are important for evaluating reservoir stability. The interbedded formation of HBS is common in target mining reservoirs. Existing studies on the triaxial mechanical properties of HBS are primarily based on homogeneous and isotropic samples. Therefore, the stress–strain law of the target mining reservoirs cannot be predicted accurately. In this study, a series of sediment models with interlayers of coarse and fine mineral grains were established based on the PFC3D code, and the influence of the layered distribution characteristics of sediment particles and hydrates on the macroscopic mechanical behaviour of the reservoir was comprehensively analysed. The triaxial compression simulation results indicate that the peak strength, deformation modulus, and cohesion of the layered HBS are significantly lower than those of the homogeneous model. The deformation modulus of the reservoir is mainly affected by the fine-grained layer without hydrates. When the coarse and fine grains correspond to different mineral components, the two minerals are heterogeneous in terms of their micromechanical parameters, which can further reduce the macroscopic mechanical parameters of the HBS. In addition, the layered distribution of hydrate results in significant anisotropy of the reservoir. This study constitutes a reference regarding the control mechanism of gas hydrate reservoir strength.

Keywords: layered hydrate-bearing sediments; anisotropy; triaxial compression simulation; mechanical properties

check for updates

Citation: Han, Z.; Zhang, L.; Zhou, J.; Pan, Z.; Wang, S.; Li, R. Effect of Mineral Grain and Hydrate Layered Distribution Characteristics on the Mechanical Properties of Hydrate-Bearing Sediments. *Energies* **2023**, *16*, 7366. https://doi.org/10.3390/en16217366

Academic Editor: Nikolaos Koukouzas

Received: 2 October 2023
Revised: 24 October 2023
Accepted: 30 October 2023
Published: 31 October 2023

Copyright: © 2023 by the authors. Licensee MDPI, Basel, Switzerland. This article is an open access article distributed under the terms and conditions of the Creative Commons Attribution (CC BY) license (https://creativecommons.org/licenses/by/4.0/).

1. Introduction

Natural gas hydrates are crystalline solids composed of natural gas and water under natural conditions; they constitute a new strategic alternative energy source with great commercial development value because of their many advantages, such as high safety, environmental protection, and energy efficiency [1–3]. The purpose of hydrate exploitation is to break the in situ stability conditions to promote the decomposition of hydrates and then discharge natural gas. The main mining methods include depressurization, heat shock, injection inhibitor, CO_2 replacement and solid fluidization [4]. However, the unqualified gas production rate has become an apparent factor hindering commercial hydrate development. Therefore, the reservoir stimulation strategy is particularly important. Hydraulic fracturing technology can increase the artificial fractures of hydrate-bearing sediments, which is an important exploration direction to improve the exploitation process of natural gas hydrate [5–7]. Submarine hydrate reservoirs are usually characterised by non-diagenesis and weak cementation. Hydrate decomposition can easily cause reservoir sedimentation and

deformation, leading to disasters such as wellbore collapse and submarine landslides [8–11]. In addition, the decomposition process and volume of hydrate in different rock intercalations are also different, which further increases the heterogeneity of the reservoir and the uncertainty of the mining process [12]. The mechanical parameters of gas hydrate-bearing sediments (HBS) provide the basic data for hydrate exploitation [13]. A correct understanding of the influencing factors and mechanisms of the mechanical behaviours of HBS is crucial for achieving safe and efficient development of hydrate resources.

Borehole data from multiple natural gas hydrate reservoirs indicate that their stratigraphic structures exhibit a characteristic vertically layered distribution [14,15]. The mineral compositions, grain characteristics, and hydrate occurrence mechanisms in different geological layers exhibit differences along the vertical direction [16–18]. For example, exploration data of HBS in the Indian Ocean show that an in situ core sample with a thickness of 7 cm consists of multiple layers of sand and clay [19], as shown in Figure 1. The geological characteristics of the reservoirs exhibit significant spatial heterogeneity and anisotropy [20,21]. However, existing studies on the mechanical characteristics of HBS are primarily based on the assumption of homogeneous and isotropic material characteristics, with research on layered HBS being limited [22–26]. Zhou et al. established a constitutive model for layered HBS considering the reservoir anisotropy [27]. Li et al. prepared layered samples in different orders of hydrate, kaolin, and mixed hydrate and kaolin layers. The triaxial test results indicated that when the hydrate layer was located in the centre of the sample, the sediment strength was the highest, and when the mixed layer was located in the middle, the sediment strength was the lowest [28]. Li et al. revealed the triaxial shear failure characteristics of sediments composed of two different hydrate-saturated layers based on laboratory tests. They confirmed that the stress–strain behaviour of the sample was mainly affected by the low-saturation layer [29]. The layered distribution of sediments and hydrates has an impact on the mechanical properties of reservoirs; however, current research has not formed a systematic understanding, making it difficult to accurately predict the stress–strain laws of target mining reservoirs.

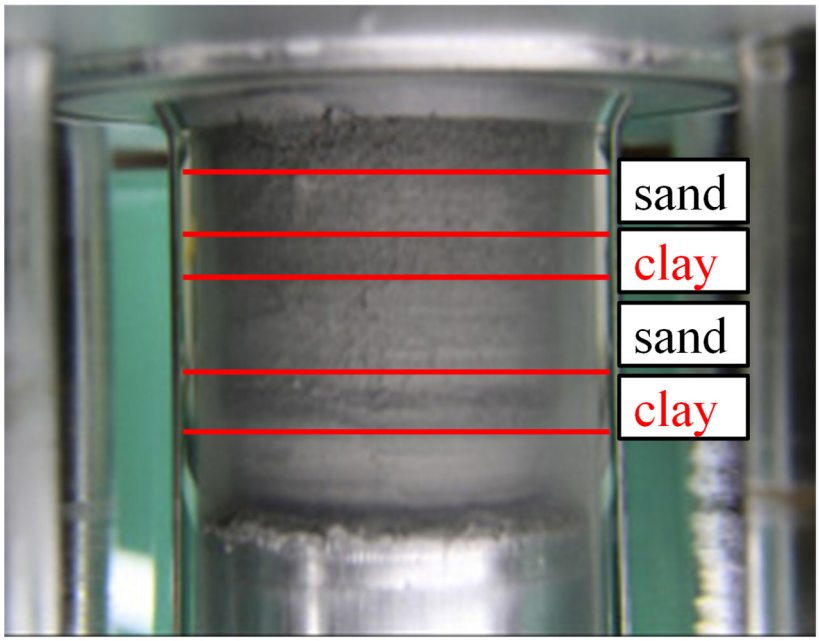


Figure 1. In situ core samples of layered HBS in the Indian Ocean [19].

Studies have shown that the mechanical properties of HBS are primarily influenced by the combined effects of sediments, hydrates, and environmental factors [30–37]. The mineral composition of the sediment has little influence on the phase equilibrium of the gas hydrate; however, the mineral grain size of the sediment determines the pore size and

is an important factor affecting hydrate saturation [38,39]. Hydrates are often found in coarse-grained sand layers, whereas adjacent fine-grained sediments contain little or no hydrates, such as the Cascadia margin [40], the Hydrate Ridge of Oregon [28], and the Shenhu Sea area in the South China Sea [41]. The grain size distribution characteristics of the sediments in the Shenhu Sea area are shown in Figure 2 [18]. The upper layer (L1) and lower layer (L3) do not contain hydrates, and the middle layer (L2) is a hydrate-bearing layer, with wider sediment grain size distribution, containing coarser components than those of layers L1 and L3. Tests have shown that the correlation between hydrate saturation and the coarse sand (>125 μm) content is best for reservoirs in the Shenhu Sea area. Sun et al. also confirmed through experiments on artificially synthesised samples containing hydrates that sediments with larger mineral grain sizes are more conducive to the occurrence of hydrates [42].

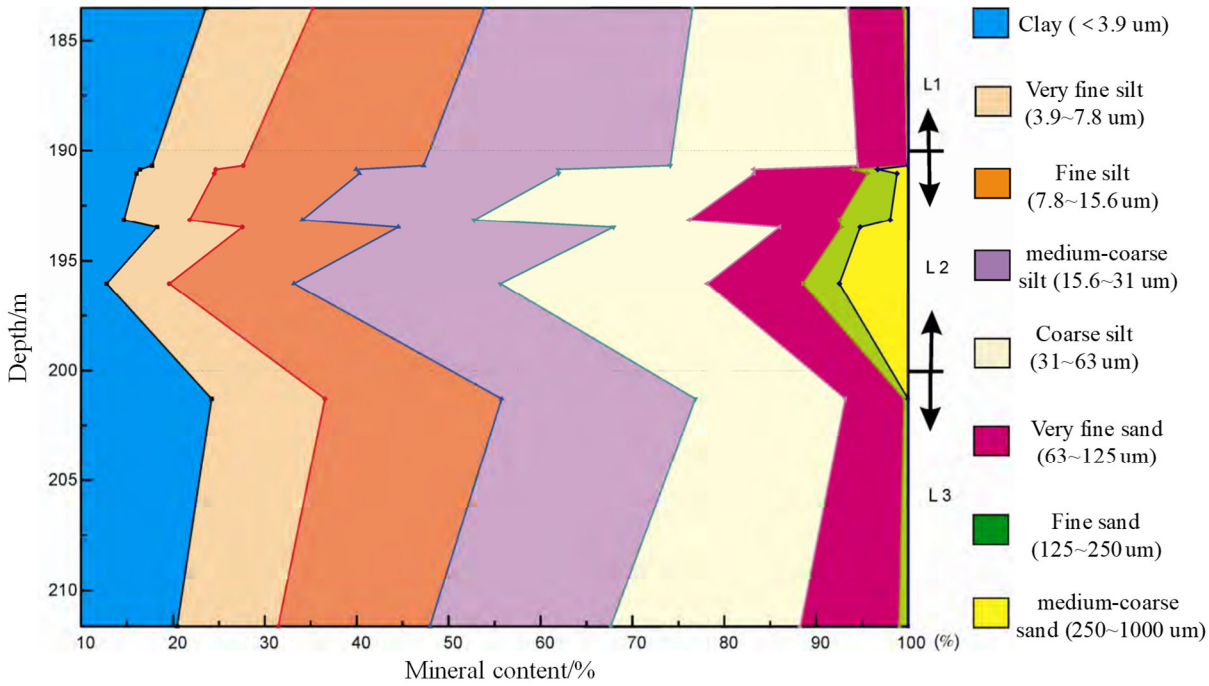


Figure 2. Grain size distribution of sediments from the Shenhu Sea area, South China Sea [18].

The distribution characteristics and physical properties of hydrates at heterogeneous and layered reservoirs differ significantly from those of artificial samples. Layered samples require accurate control of the hydrate distribution and simulating the characteristics of actual heterogeneous reservoirs through manual indoor sampling remains an urgent problem to be solved. Therefore, this study adopted the PFC three-dimensional discrete element simulation method. In the numerical model, sediment particles and hydrates were stratified based on the differences in mineral grain sizes. The influence of the layered distribution characteristics of sediment particles and hydrates on the macroscopic mechanical properties of the HBS was analysed using a series of triaxial compression simulations.

2. Modelling Methodology and Scenarios

2.1. Methodology

In this study, PFC3D code was used to simulate the mechanical behaviours of HBS, which is based on the distinct element method (DEM). The PFC code uses particle aggregates to characterize materials [43]. The non-continuous mechanical behaviours of the HBS can be reflected by simulating the interactions and movements of mineral and hydrate particles [44]. In PFC code, the fundamental relationships between particle motion and the forces causing that motion are Newton's second law and the force-displacement law. The interaction between particles is a dynamic process. When the internal force is balanced, the

equilibrium state will develop [43]. The relationship between the contact force between the particles and the relative displacement needs to meet Equations (1) and (2), since the shear force is related to the particle motion and the stress path, which is expressed in an incremental form.

$$F^n = K^n U^n \tag{1}$$

where F^n is the normal contact force. K^n is the normal stiffness at the contact. U^n is the relative contact displacement in the normal direction.

$$F_i^s = -F_{i-1}^s + K^s U^s \tag{2}$$

where F_i^s is the shear contact force. K^s is the shear stiffness at the contact. U^s is the relative contact displacement in the shear direction.

PFC provides two basic contact models: parallel bonded and contact bonded (Figure 3). The parallel bonded model can be assumed as a cemented polymer, which can transmit both a force and a moment, while the contact bond can transmit only a force. Because hydrates have a significant cementation effect on sediment particles, the model achieved the cementation effect of hydrates by using the parallel bonded mode between hydrate particles and sediment particles [3]. When there was no hydrate interaction between sediment particles, the contact bonded model was used.

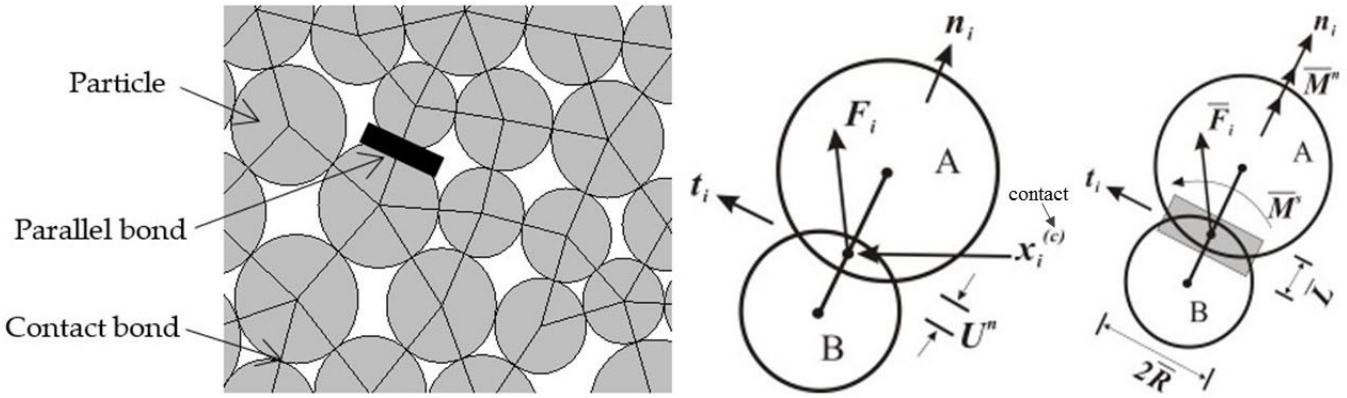


Figure 3. Force–displacement behaviour of the particle bonding system [3].

2.2. Model Description

A cubic specimen with a side length of 5 mm was used for triaxial compression simulation. Stress boundary conditions were applied to the six walls. The particles were fully consolidated under a fixed confining pressure and the loading process was simulated by controlling the movement of the upper and lower boundaries using a servomechanism. When the axial strain value reaches 0.15, the loading process will stop. The mineral grain size, porosity, and hydrate saturation of the model were determined using the HBS from site SH3, Shenhu Sea area, South China Sea. The survey showed that the pores in the Shenhu Sea area are relatively uniform, with porosities ranging from 33% to 55% [18]. The maximum hydrate saturation of the sediment measured in situ at site SH3 was 25.5%. Hydrates are mainly produced in very fine silt and coarse sand layers, and the grain size range of sand sediments varies greatly (3.9 μm–1.0 mm) [18,45,46]. In the simulation, the porosity and hydrate saturation of the model were assumed to be 45% and 20%, respectively. The formation of hydrates in this model is illustrated in Figure 4. The sediment particles are granular materials, and when they are in contact with hydrate particles, a bonding effect occurs at the contact position.

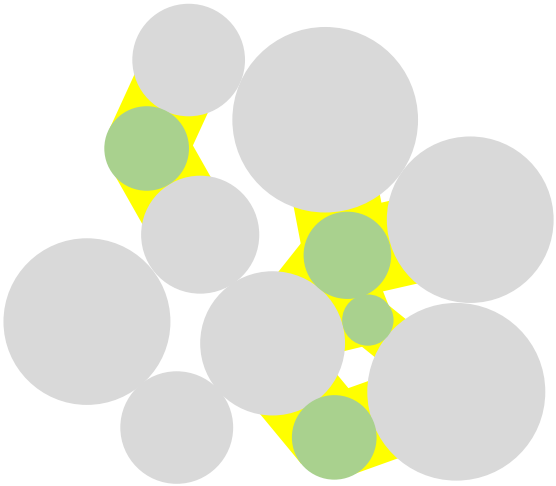


Figure 4. Characterization of sediment particles and hydrate particles in the model (grey: sediment particles; green: hydrate particles; yellow: parallel bonded).

2.3. Modelling Scenarios

The aim of this study was to investigate the effects of the layered distribution characteristics of sediment particles and hydrates on the macroscopic mechanical properties of HBS. Factors such as mineral grain size, mineral micromechanical parameters, layering characteristics, and hydrate distribution were considered. To simulate the layering effect of the sediment, the model consisted of two mineral grain layers with significantly different grain sizes. As mentioned earlier, the correlation between hydrate saturation and the coarse sand (0.25–1.00 mm) content was increased. Therefore, the grain size range of the coarse-grained mineral was set to 0.25–0.40 mm, and the grain size range of the fine-grained mineral was set to 0.16–0.20 mm, while considering the model's computational efficiency. In the model, hydrates were mainly present in the pores of coarse-grained mineral. Therefore, the grain sizes of the hydrate particles were small; otherwise, it would be difficult to generate sediment samples that meet the set saturation value (20%). However, small hydrate particles inevitably lead to a sharp increase in the number of model particles, thereby greatly reducing the technical efficiency. Therefore, considering the above two factors, the particle size of hydrate was set to 0.10–0.12 mm. The specific scenarios are as follows (Table 1):

(1) Layered models that consider mineral grain size differences

Table 1. Three scenarios with different sedimentary layer distribution characteristics.

Scenario	Model	Influence Factors	Confining Pressure/MPa
1	A, B, C, D	Mineral grain and hydrate layered distribution, hydrate saturation	1, 2, 3
2	A, B, C, D	Mineral grain and hydrate layered distribution, material heterogeneity	1, 2, 3
3	C	Anisotropy of the HBS	1

In scenario 1, four different sediment distribution models were designed. The content and porosity of different mineral grains in the four models were consistent, which were different from the distribution of two mineral grains and hydrates. As shown in Figure 5, model A represented a homogeneous model, in which coarse and fine grains were uniformly distributed, and hydrates were also uniformly distributed in the pores of mineral grains. Models B, C, and D were layered models with interlayered coarse and fine grains, and the hydrates were distributed only in the pores of the coarse grains. Usually, the higher the number of layers, the closer the model is to the homogeneous model. In model B, the

sediment was divided into six layers; in models C and D, the sediments were divided into four and two layers, respectively, to explore the impact of the number of layers on the HBS. In addition, to distinguish between the effects of mineral grain layering and hydrate layering, scenario 1 considered two types of hydrate saturation: 0% and 20%.

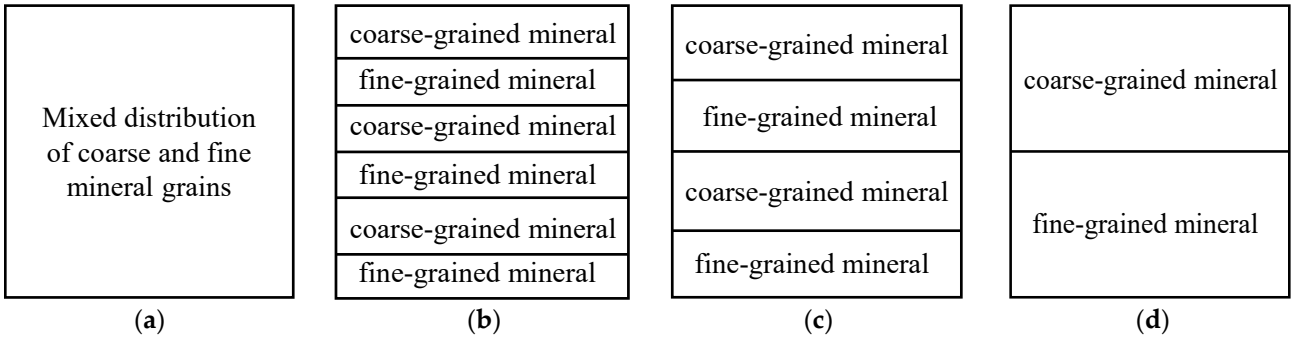


Figure 5. Four different sediment particle models. (**a**) Homogenous model A; (**b**) six-layer sediment model B; (**c**) four-layer sediment model C; (**d**) two-layer sediment model D.

(2) Layered model scenarios considering differences in mineral micromechanical parameters

For models containing hydrates (Sh = 20%), to clarify the effect of sediment layered characteristics on the mechanical behaviour of HBS, two comparison scenarios for microparameters were designed. In scenario 1, the two minerals in models A to D adopted the same microparameters shown in Table 2, which are the average values of the coarse and fine mineral microparameters. In scenario 2, different micromechanical parameters were used for the coarse and fine minerals, as listed in Table 2. Thus, the mechanical behaviour of the model was also influenced by the heterogeneity of the mineral micromechanical parameters.

Table 2. Micro-physical and mechanical parameters in numerical modelling.

	Microparameters	**Hydrate**	**Parameters for Scenario 2**		**Parameters for Scenario 1**
			Coarse Grain	**Fine Grain**	**Average Value of Coarse and Fine Grain**
Particle	Density/kg/m^3	300	2500	2500	2500
	Modulus/MPa	50	150	50	100
	Normal-to-shear stiffness	1.5	1.5	1.5	1.5
	Friction coefficient	0.5	0.8	0.2	0.5
Parallel bond	Tension strength/MPa	3			
	Shear strength/MPa	3			
	Normal-to-shear stiffness	1.5			
	Modulus/MPa	50			
	Friction coefficient	0.5			

(3) Layered model scenarios considering anisotropy of the HBS

In scenario 3, the anisotropy of the HBS was analysed by changing the dip angle β of the bedding plane, using model C as an example. As shown in Figure 6, the bedding dip angle was set to 0°, 10°, 45°, 60°, and 90°.

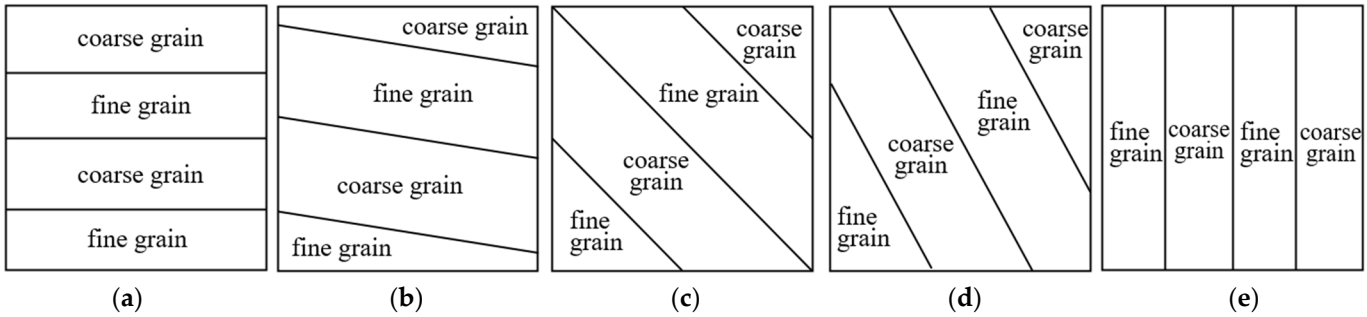


Figure 6. Sediment particle models with different bedding dip angles (taking model C as example). (**a**) β = 0°; (**b**) β = 10°; (**c**) β = 45°; (**d**) β = 60°; (**e**) β = 90°.

In addition, to obtain the cohesion and internal friction angle of the model, three confining pressure conditions were considered, namely 1, 2, and 3 MPa.

2.4. Microparameter Calibration

In this simulation, the microscopic parameters of the numerical model were inverted based on the experimental results [3,47]. Owing to limitations in the experimental conditions, no corresponding experimental research was conducted in this work. Therefore, the microparameters of this simulation mainly refer to parameter values from existing studies. By adjusting the microparameters, the simulated macroscopic mechanical parameters were within reasonable ranges for the mechanical parameters of the HBS in the Shenhu Sea area, South China Sea. Wang et al. synthesised HBS samples using sediment particles from the Shenhu Sea area and conducted triaxial compression tests [46,48]. For hydrate saturation in the range of 18–26% and where the confining pressure is 1 MPa, the macroscopic parameters of the sample based on their test results are listed in Table 3. The microparameters of the sediment and hydrate particles were calibrated based on the experimental results of Wang et al. [46,48] as shown in Table 2. The macroscopic mechanical parameters of the simulation were within a reasonable range (as shown in Table 3) to ensure the reliability of the microscopic parameters. As shown in Table 2, the average values of the coarse and fine mineral parameters were used in scenario 1, and different parameters were used in scenario 2. A detailed analysis of the simulation results is presented in the following section.

Table 3. Macro-mechanical properties comparison between experimental and simulated HBS results.

Macro-Mechanical Properties	Experimental Results	Simulated Results
Peak strength/MPa	0.9–3.5	2.1–4.0
Elastic modulus E_{50}/MPa	40–150	50–75
Cohesion/MPa	0.2–0.9	0.5–0.9
Internal friction angle/°	20–25	20–25

3. Influence of Layered Distribution of Sediments and Hydrates

According to scenario 1, four particle distribution models with different sedimentary layers and hydrate saturations were established, as shown in Figures 7 and 8. The models shown in Figure 7 did not contain hydrates, and involved differences only in the mineral grain sizes between different layers. The layering effect of the mineral grains was analysed based on the simulation results. The models shown in Figure 8 contained hydrates with a saturation of 20%, with their mechanical behaviours being affected by both mineral grains and hydrate layering. With an increasing number of layers, the model approached a homogeneous sample condition. To better describe the relationship between the number of layers and the macroscopic parameters of the model, a layer thickness ratio n was defined to characterize the layering of sediment particles and hydrates, as shown in Equation (3).

$$n = h/H \tag{3}$$

where h represents the single-layer thickness of the sediment model and H represents the total height of the model. Owing to the absence of layering in model A, the layer thickness ratio n was zero. As the number of layers decreased, n gradually increased. When the number of layers was two, the layer thickness ratio n reached a maximum value of 0.5. In this scenario, the coarse and fine mineral grains adopted the same micromechanical parameters, and the layering effects of the mineral grains and hydrates were analysed based on the modelling results.

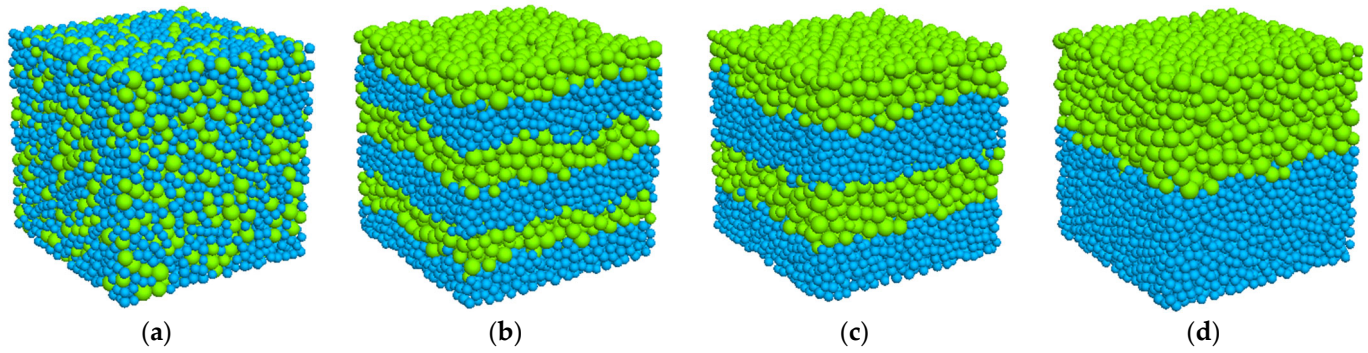


Figure 7. Numerical models with different sedimentary layers without hydrates (green: coarse grain; blue: fine grain). (**a**) Model A, n = 0.00; (**b**) model B, n = 0.17; (**c**) model C, n = 0.25; (**d**) model D, n = 0.50.

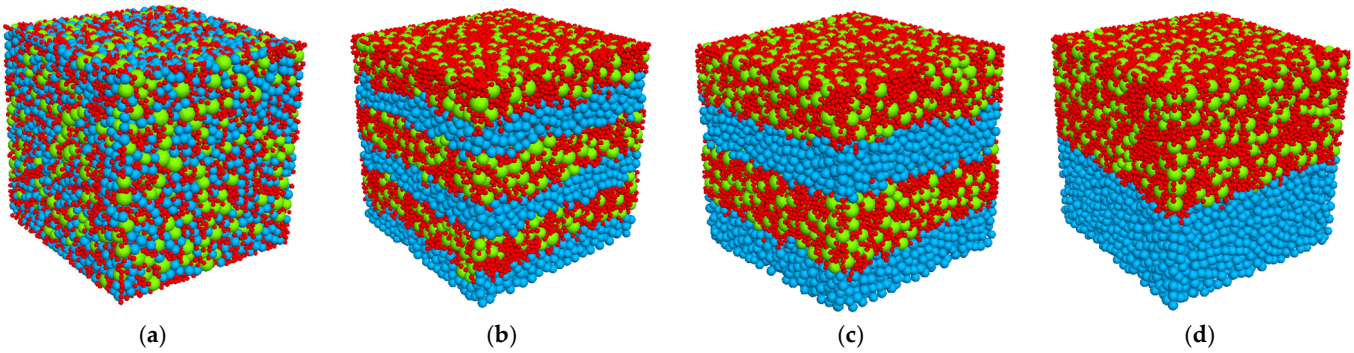


Figure 8. Numerical models with different sedimentary layers with hydrate saturation of 20% (green: coarse grain; blue: fine grain; red: hydrate). (**a**) Model A, n = 0.00; (**b**) model B, n = 0.17; (**c**) model C, n = 0.25; (**d**) model D, n = 0.50.

3.1. Effects of Sediment and Hydrate Layering on Deviatoric Stress-Strain Curves

The stress-strain relationship of HBS is the basis for evaluating reservoir strength and deformation parameters. Triaxial compression simulations were conducted based on the models shown in Figures 7 and 8 under different confining pressure conditions. The deviatoric stress–strain curves of the models with different layer thickness ratios n and hydrate saturations under a confining pressure of 1 MPa are shown in Figure 9. The deviatoric stress–strain curves of the models without hydrates were characterised by strain hardening because the sediment particles in the models were relatively loose. As the strain increased, the deviatoric stress approached a constant value. However, when the models contained hydrates, the deviatoric stress–strain curves exhibited clear strain softening characteristics. The main reason for this is that the hydrates have significant cementation and support effects on the sediment particles. When the sample reaches the yield state, the cementation of the hydrate between sand particles fails, some particles cross the adjacent particles, and the local density of the model becomes loose, which causes a strain softening phenomenon. Figure 9 shows that the difference in peak strength among the four models without hydrates is very small, and in all cases around 1.0 MPa. Additionally, the modulus

during the elastic deformation stage was almost the same, indicating that the layering of sediment particles had little effect on the peak strength and elastic modulus. When the models contained hydrates, the strength and modulus increased significantly, and the layered occurrence of hydrates also affected the macroscopic mechanical parameters of the model. The peak strength and deformation modulus of model A were significantly higher than those of models B, C, and D.

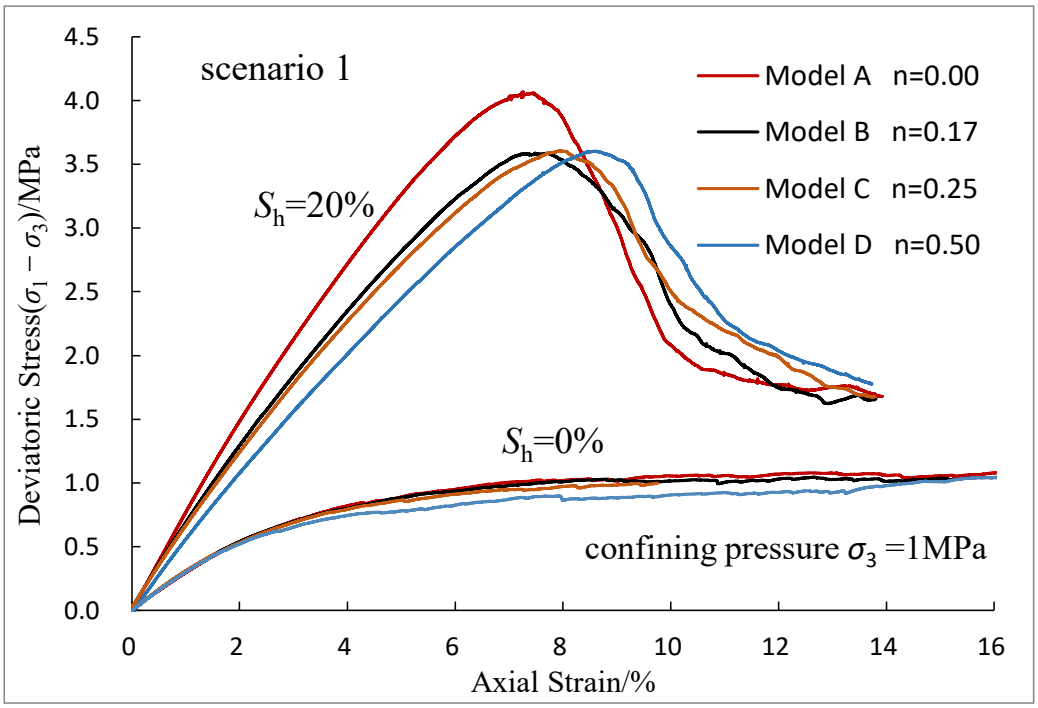


Figure 9. Deviatoric stress–strain curves of models with different layer thickness ratios under confining pressure of 1 MPa in scenario 1.

3.2. Effects of Sediment and Hydrate Layering on Peak Strength and Deformation Modulus

The layering of sediment particles had little effect on the peak strength and deformation modulus without the effect of hydrates. Hence, this study mainly analysed the impact of hydrate layering, as shown in Figure 10, where the peak strength of the homogeneous hydrate model A was significantly higher than those of the layered samples, whereas the peak strengths of models B, C, and D were basically the same. This demonstrates that the layered distribution of hydrates reduced the peak strength of the HBS, whereas the number of layers had little effect on the peak strength of the HBS. This was mainly because the mineral grains in Model A were uniformly cemented by the hydrates to form a well-formed structure. During the triaxial compression process, this cementation restricts the relative motion—such as rolling, sliding, and rotation—of mineral grains, resulting in a higher macroscopic strength of the sediment. However, in models B–D, the hydrates were only distributed in the coarse-grained mineral layer, and the fine-grained mineral layer remained in a dispersed state. The content of the fine-grained mineral layer without hydrates affected the overall strength of the model. Owing to the same proportion of fine-grained minerals in models B–D, there was no significant difference in peak strength. Li et al. also confirmed that the hydrate-free layer content has a controlling effect on strength by experiments and numerical simulations [29].

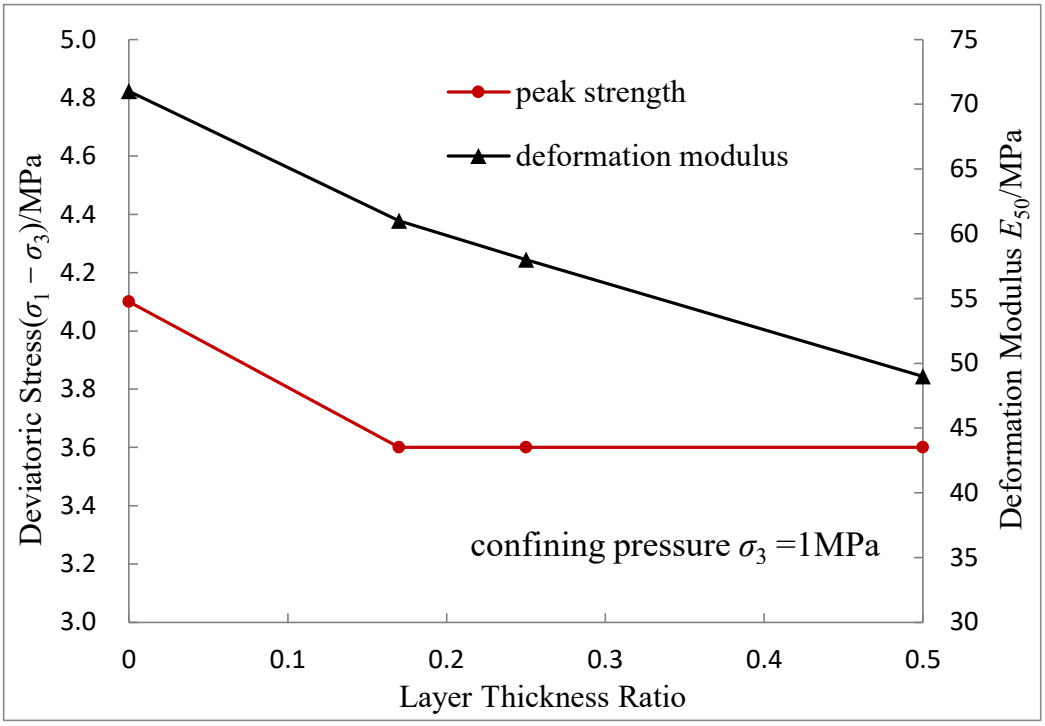


Figure 10. Effects of the layer thickness ratio of the hydrates on the model peak strength and deformation modulus under confining pressure of 1 MPa.

Figure 10 also shows that the layered distribution of the hydrates had a significant impact on the deformation modulus of the HBS. In this study, while referring to existing literature [3,29,31], the secant modulus E_{50} was used to characterize the deformation modulus of the model. The homogeneous sample had the highest deformation modulus, and as the layer thickness ratio increased, the deformation modulus gradually decreased. When the layer thickness ratio was increased from 0.0 to 0.5, the deformation modulus E_{50} decreased by 31%. A linear relationship between the deformation modulus E_{50} and thickness ratio n was obvious (R^2 = 0.98), which can be expressed by Equation (4).

$$E_{50} = -43.1n + 69.6 \ (0 \leq n \leq 0.5) \quad (4)$$

In the PFC code, the sediment particles were simulated as rigid bodies, with the axial deformation mainly originating from the compression of the pores, followed by a small deformation at the contact position between the particles. The compressibility of the coarse-grained mineral layer was higher than that of the fine-grained mineral layer because the coarse-grained minerals were cemented together by the hydrates. Therefore, the spatial distribution of the fine-grained mineral layers without hydrates is a key factor affecting the deformation modulus. When coarse and fine grains are interlayered, cementation of hydrates also occurs at the upper and lower interfaces of the fine-grained mineral layer, which can enhance the ability of the fine-grained mineral layer to resist deformation. As shown in Figure 8, a greater number of layers results in a larger proportion of fine grains cemented by hydrates with the same model size, and the deformation modulus of the model also increases accordingly (Figure 10). In model D, the proportion of compressible pores was the largest and its deformation modulus was the smallest.

3.3. Effects of Sediment and Hydrate Layering on the Internal Friction Angle and Cohesion

Cohesion and the internal friction angle are important factors affecting the shear strength of HBS. The internal friction angle is also an important engineering parameter for predicting submarine landslides. These two mechanical parameters were calculated based on the simulation results under the three confining pressure conditions. Taking models

A and D containing hydrates as examples, Figure 11 shows the deviatoric stress–strain curves of the models under confining pressures of 1 and 3 MPa. As the confining pressure increased, the peak strength and deformation of the model also increased significantly, which is consistent with existing experimental results [49,50]. The main reason for this is that an increase in the effective confining pressure limits the free movement of particles and enhances the friction between particles, thereby improving the strength and resistance to deformation of the model. The influence of the confining pressure on the mechanical properties of HBS has been extensively studied in previous research, and this article will not elaborate further. In this study, Mohr's stress circles and strength envelopes were drawn according to the simulation results to obtain the variations in the internal friction angle and cohesion with the layer thickness ratio.

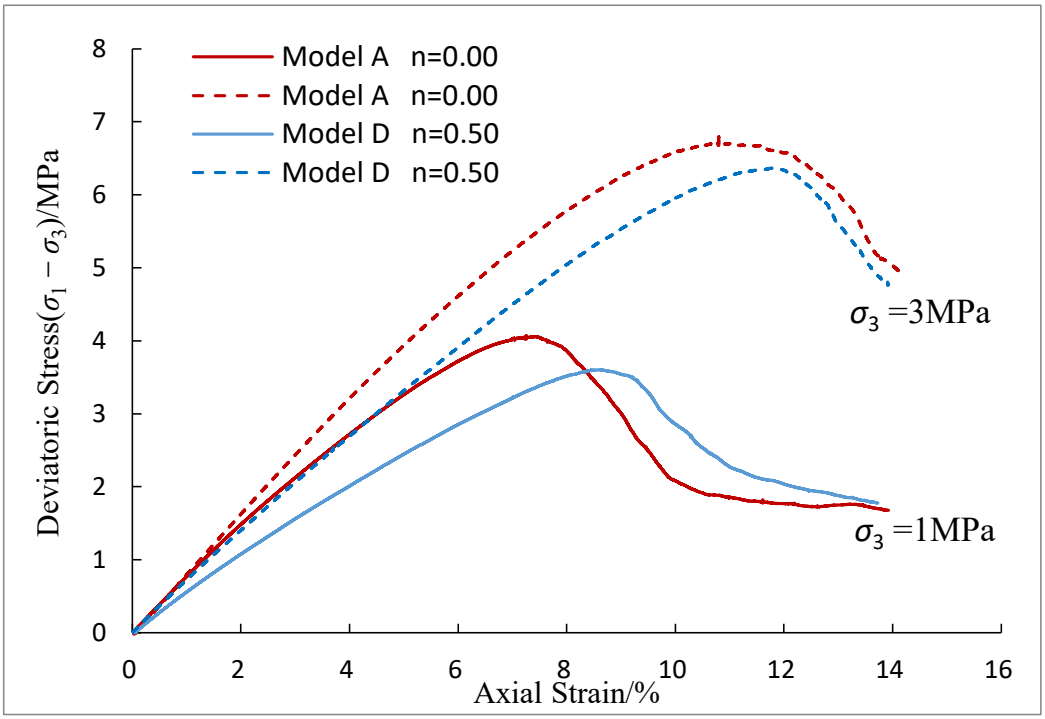


Figure 11. Comparison of deviatoric stress-strain curves of models under confining pressures of 1 and 3 MPa (taking models A and D as examples).

Taking model C (n = 0.25) containing hydrates as an example, Mohr's stress circles and strength envelopes of the model are shown in Figure 12. The angle between the common tangent and the σ-axes represents the internal friction angle, and the τ value at the intersection of the common tangent and the τ-axis is the cohesion. The variations in the cohesion and internal friction angle with different hydrate saturations and layer thickness ratios are shown in Figure 13. In the absence of hydrates, the models did not have cohesion due to the lack of bonding between sediment particles. Hydrates could significantly improve the cohesion of the models, and the layering of hydrates also affected the cohesion (Figure 13). The cohesion of homogeneous model A was 0.9 MPa, whereas the difference in cohesion between the layered samples was very small, with values being close to 0.6 MPa. Because the sediment particles used in the model were loose materials, the cohesion of the model was mainly due to the bonding effect of the hydrates on the sediment particles. In this study, although the hydrate saturation values of the four models were the same, differences in cohesion persisted, indicating that the formation of hydrates also had an impact on cohesion. Model cohesion under uniform hydrate occurrence was higher than that under layered conditions.

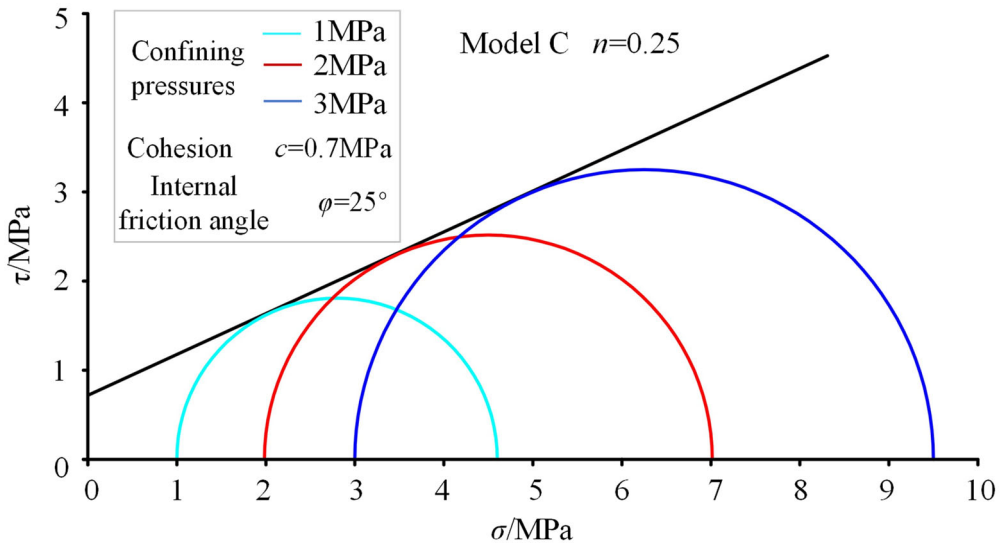


Figure 12. Mohr's stress circles and the strength envelopes of model C.

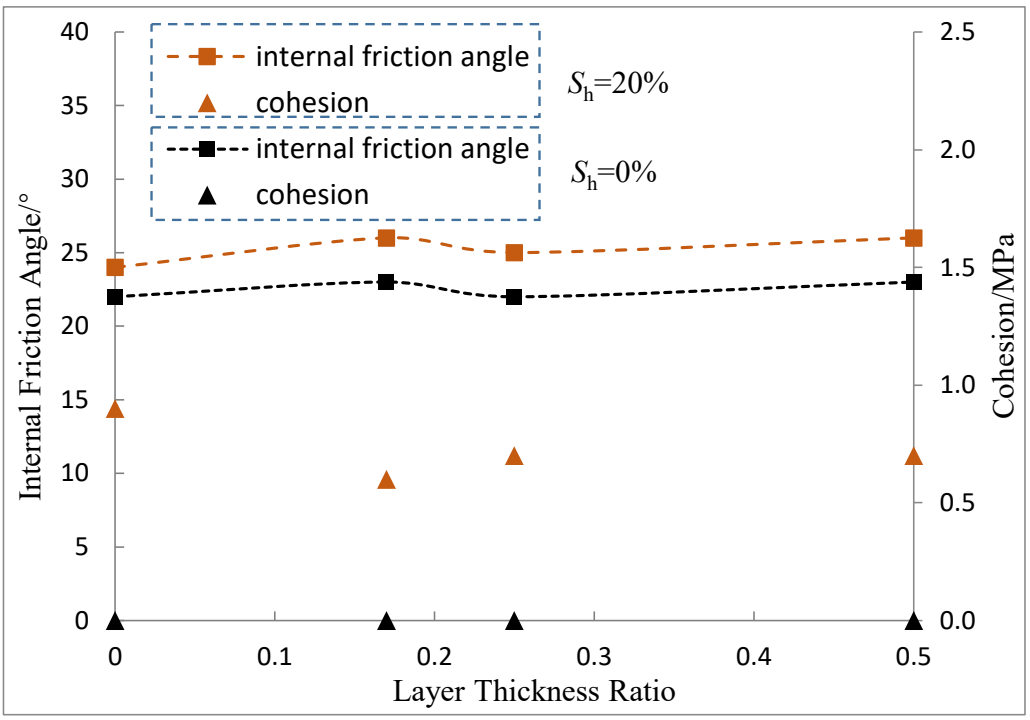


Figure 13. Effects of the layer thickness ratio and hydrate saturation on model cohesion and internal friction in scenario 1.

Figure 13 also shows that the layering of mineral grains and hydrates had little impact on the internal friction angle, whereas the increase in hydrate saturation had an increasing effect on the internal friction angle; however, the effect was not very significant. The internal friction angle of the model without hydrates was approximately 22°, whereas with hydrate saturation of 20%, it was approximately 25°, i.e., it increased by approximately 12%. The internal friction angle of the HBS was mainly determined by the frictional resistance generated by the model particles under pressure. In scenario 1, the friction coefficient between particles was the same in the different models; thus, their internal friction angles were essentially the same. Hydrates have little effect on the bite force generated by surface friction between sediment particles; therefore, the influence of hydrates on the internal friction angle is very limited.

4. Influence of Material Heterogeneity on Mechanical Property of HBS

In scenario 2, for the four models shown in Figure 8, different micromechanical parameters were adopted for the coarse and fine grains, and the differences were mainly reflected in the particle modulus and friction coefficient. As shown in Table 2, the modulus and friction coefficient of the coarse particles were higher than those of the fine particles, leading to material heterogeneity in different sedimentary layers.

Triaxial compression simulations were conducted on the four models in scenario 2 under different confining pressure conditions. Taking confining pressure of 1 MPa as an example, the deviatoric stress–strain curves of the models are shown in Figure 14, exhibiting obvious strain-softening characteristics, which are similar to those of the models containing hydrates in scenario 1. The variations in the peak strength and deformation modulus with the layer thickness ratio were obtained according to these curves, as shown in Figure 15a. The deformation modulus of the model still had a good correlation with the layer thickness ratio ($E_{50} = -36.9n + 64.0$ $R^2 = 0.94$). Compared with scenario 1, the strength and modulus of the HBS were significantly reduced when the material heterogeneity of the sediment particles was considered. The comparison of Figures 9 and 14 shows that, in scenario 1, when the strain reached between 7.5% and 9.0%, the four models reached the peak stress. After considering material heterogeneity in scenario 2, the model reached its peak strength when the strain was between 6.5% and 8.0%. This was mainly because the material heterogeneity of the mineral grains increased the local deformation disharmony and stress concentration, thereby accelerating the failure of the model. The variations in the cohesion and internal friction angle with the layer thickness ratio are shown in Figure 15b. Compared with scenario 1, the increase in material heterogeneity reduced the model internal friction angle; however, the effect on cohesion was not significant, further confirming that model cohesion was mainly affected by the hydrates.

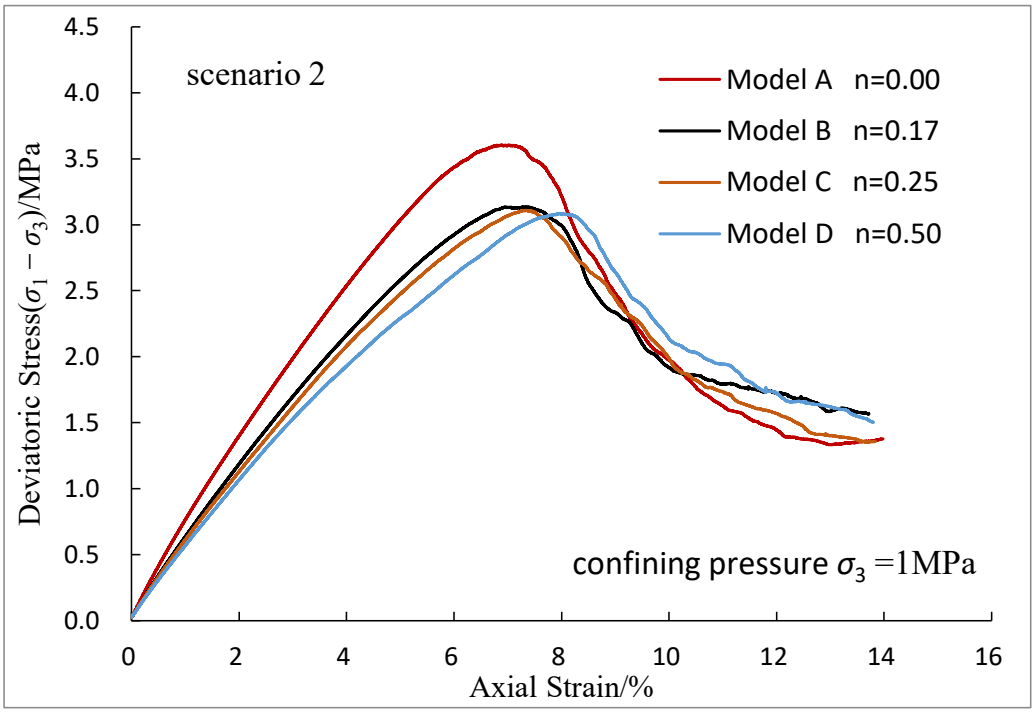


Figure 14. Deviatoric stress–strain curves of models with different layer thickness ratio under confining pressure of 1 MPa in scenario 2.

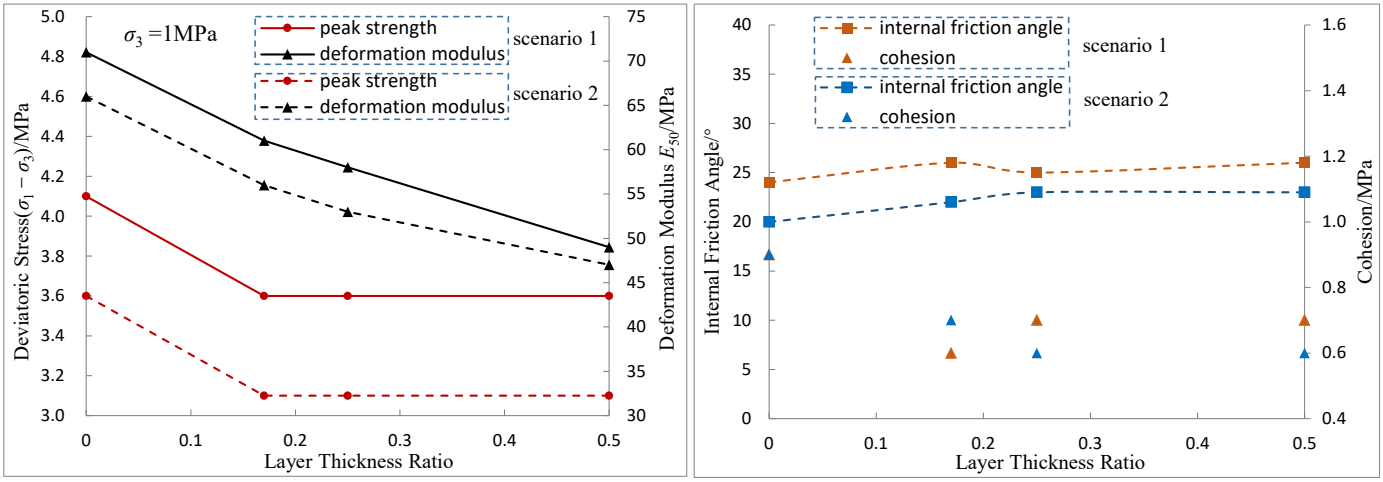


Figure 15. Effects of material heterogeneity on the model macro-mechanical parameters in scenario 2. (**a**) Peak strength and deformation modulus and (**b**) cohesion and internal friction angle.

5. Influence of Anisotropy on the Mechanical Properties of HBS

Anisotropy is an inherent attribute of layered HBS and is also a key factor affecting the stability of hydrate reservoir wellbores. To investigate the impact of anisotropy on the macroscopic mechanical behaviour of HBS, triaxial compression simulations of model C containing hydrates at different bedding dip angles were conducted in scenario 3. The numerical models with different bedding dip angles are shown in Figure 16. The effects of anisotropy on the macroscopic mechanical parameters and microcrack evolution of the model were analysed based on the simulation results.

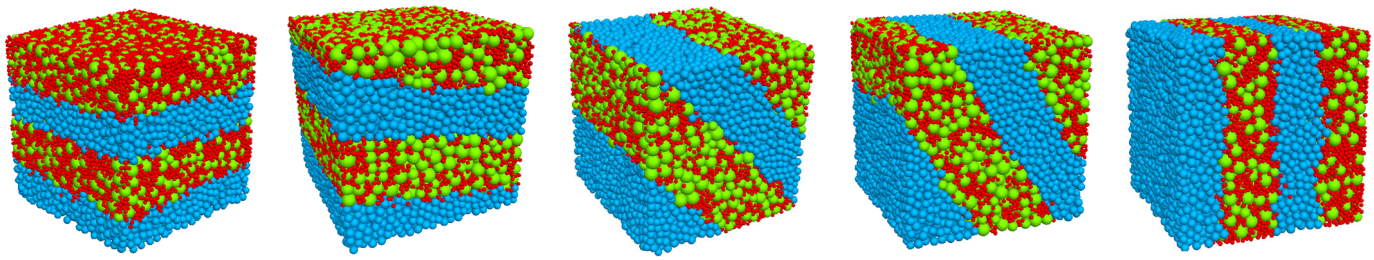


Figure 16. Sediment particle models with different bedding dip angles (green: coarse grain; blue: fine grain; red: hydrate). (**a**) 0°, (**b**) 10°, (**c**) 45°, (**d**) 60°, and (**e**) 90°.

The variations in the peak strength and deformation modulus with the bedding dip angle were obtained, as shown in Figure 17. Figure 18 shows the distribution of microcracks inside the model when the axial stress reached 90% of the peak strength in the post-peak stress stage. Microcracks represent the failure of the parallel bond between the hydrate and sand particles; therefore, microcracks exist only in the layers containing hydrates. In Figure 17, as the bedding dip angle β increases from 0° to 90°, the peak strength of the models first decreases and then increases, with the minimum value obtained at dip angle of 60°. The variation in peak strength with the inclination angle of the bedding plane was related to the stress state of the model particles. Because the strength at the intersection of each layer was relatively low, formation was easy through cracks that were consistent with the bedding dip angle within a certain angle range (β = 45–60°), as shown in Figure 18c,d, in which case the model peak strength was the smallest. When the dip angle of the bedding plane approached 0° or 90°, the model involved many microcracks, which were, however, difficult to penetrate; hence, the macroscopic fracture zone was wider (Figure 18a,b,e),

resulting in high model strength. Figure 17 shows that the deformation modulus gradually increases with an increase in the bedding dip angle. As mentioned earlier, the fine-grained mineral layer without hydrates is a key factor affecting the deformation modulus of the model. When the dip angle of the bedding plane was 90°, the coarse-grained mineral layers containing hydrates ran through the entire model along the axial compression direction, thereby limiting the compression of the fine-grained mineral layers on both sides, resulting in the maximum deformation modulus. As the bedding dip angle decreased, this limiting effect weakened, and the deformation modulus gradually decreased. When the angle decreased to 0°, the fine-grained mineral layers could be freely compressed in the axial compression direction, with the deformation modulus being at a minimum.

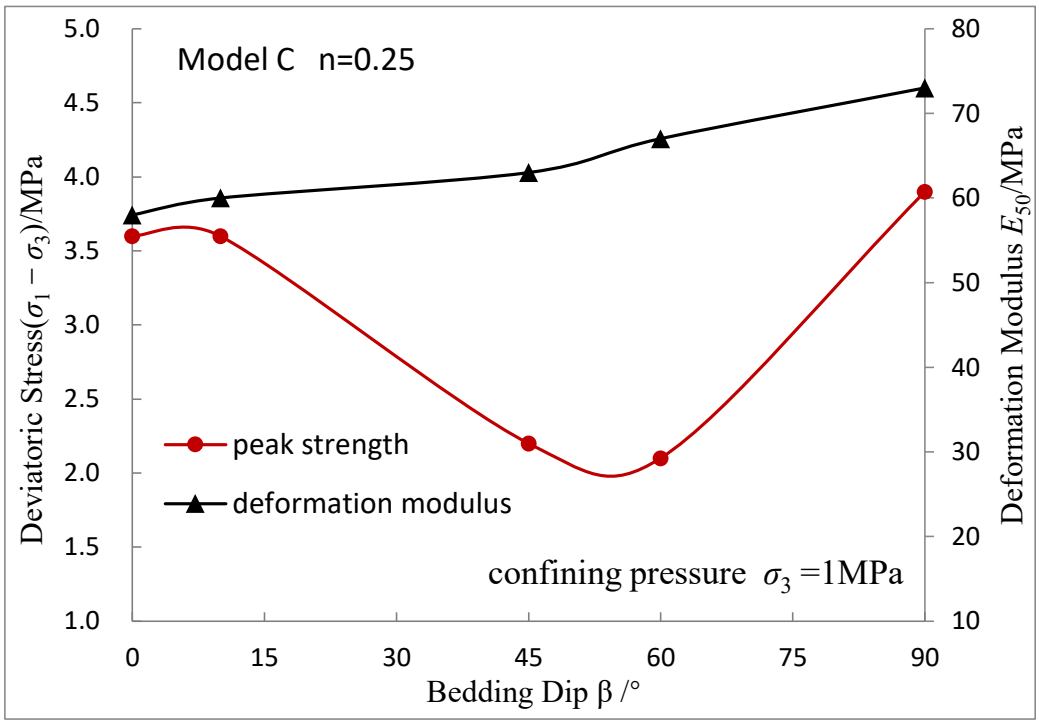


Figure 17. Effects of anisotropy on model peak strength and deformation modulus under confining pressure of 1 MPa.

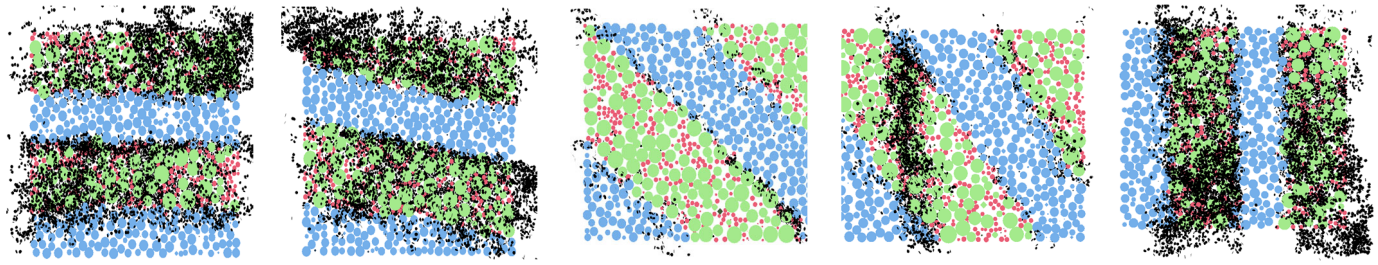


Figure 18. Microcrack distributions of sediment particle models with different bedding dip angles (black: microcrack; green: coarse grain; blue: fine grain; red: hydrate). (**a**) 0°, (**b**) 10°, (**c**) 45°, (**d**) 60°, and (**e**) 90°.

6. Discussion

Layered sediments are common in hydrate mining areas. On-site logging data show that layered HBS in the reservoirs are mainly formed by horizontal overlapping of thin layers with thicknesses of several centimetres. The layered distribution characteristics of the sediments and hydrates have a significant impact on the physical and mechanical

properties of HBS, mainly manifested in three aspects. First, seabed sediments have a characteristic vertical layered distribution, with the mineral sizes or components being different in different layers, thereby affecting the mechanical properties. Second, affected by the mineral grain size differences, hydrate saturation varies in different layers, thereby further affecting the mechanical properties of HBS. Third, the layering of sediments and hydrates results in significant anisotropy in the mechanical properties of HBS. Sediment features affect the generation and occurrence of natural gas hydrates in the pores, and the sediment grain size plays a major role. Therefore, two mineral grains with obvious differences in grain size were used in this study, and a layered sediment model was established in the form of interbedded coarse and fine mineral grains. Based on the actual occurrence habits of the hydrate, it was distributed in the pores of the coarse-grained layer of the model.

Based on the simulation results, if the coarse and fine mineral components are the same, the layering characteristics of the sediments caused by grain size differences have little impact on their mechanical parameters. The content and layered distribution characteristics of the hydrates control the mechanical properties of HBS. Natural gas hydrates in marine areas are generally found in loose sedimentary layers with high porosity, having an obvious cementation effect on the sediments. Under a layered distribution of hydrates, the cementation effect of the hydrates on sediment particles in different sublayers is different, resulting in heterogeneity of the strength, stiffness, and local shear deformation characteristics of the sediments. Therefore, the strength, deformation modulus, and cohesion of the hydrate-layered distribution model are significantly lower than those of the homogeneous model, and the failure mechanism is more complex.

If the mineral composition of sediments at different layers is different, that is, when mineral grains with obvious differences in mechanical properties are deposited in the interlayer, the superposition of the hydrate-layering effect and heterogeneous material effect further reduces macroscopic parameters such as the strength and modulus of sediments. Comparing the simulation results of scenarios 1 and 2, after considering the material heterogeneity, the peak strength, deformation modulus, and internal friction angle can be reduced by 25%, 35%, and 20%, respectively. In fact, the phenomenon of interlayer deposition of different mineral components, such as clay and sand, is common in hydrate reservoirs. During hydrate mining, depressurization and hydrate decomposition may lead to stress redistribution and deformation of the sedimentary layer, which are not conducive to safe exploitation. If the macroscopic mechanical parameters obtained from homogeneous sample testing are used to evaluate the stability of reservoirs, the mechanical strength will be overestimated. Therefore, the layered characteristics of the sediments and the mineral heterogeneity effect are worthy of attention in comprehensive evaluations of reservoir stability.

This study also indicates that anisotropy has a significant influence on the mechanical behaviour of HBS. Compared with that of the homogeneous samples, the peak strength of the inclined-layer samples can be reduced by up to 50%. The geological conditions of the seabed are complex, and hydrates are closely related to typical sedimentary structures, such as faults, folds, and diapiric structures. Owing to the influence of tectonism, the seabed strata are not absolutely horizontal, and local sedimentary strata may exhibit large dip angles, particularly in areas where folds, high-angle faults, and vertical fractures, which are also the main fluid migration channels for hydrate accumulation and enrichment, develop. Therefore, because of the influence of stratigraphic anisotropy, there are differences in the mechanical properties of reservoirs in different mining areas. When evaluating reservoir strength, the anisotropic effect of sediment formation cannot be ignored.

In summary, the layering effect of sediments and hydrates can be described as follows. The difference in mineral grain size results in layered characteristics of sediments, with hydrates preferentially occurring in the coarse-grained mineral layers, resulting in a layered distribution of hydrates. Owing to the layering of hydrates, there is significant material heterogeneity in the sediments at different layers, thereby affecting the macroscopic me-

chanical properties of HBS. When coarse and fine grains are mineral components with different mechanical properties, the heterogeneity of the materials in different layers is further enhanced, resulting in further decreases in the macroscopic mechanical parameters of HBS. Additionally, the layered distributions of mineral grains and hydrates result in significant anisotropy in the mechanical characteristics of the sediments. These findings provide significant guidance for promoting the safe exploitation of natural gas hydrates.

7. Conclusions

Existing studies on the mechanical properties of HBS are mostly based on homogeneous materials. In this study, the layered model was established based on the PFC3D code with reference to the real distribution characteristics of the reservoir. The effects of the layered distribution characteristics of sediment particles and hydrates, material heterogeneity, and anisotropy on the triaxial compression mechanical properties of HBS were investigated. Based on the simulation results, the main conclusions are as follows:

(1) The layered distribution of hydrates has a significant impact on the mechanical behaviour of HBS. Compared with the homogeneous model, the layering of the hydrates reduces the peak strength and cohesion of the sample; however, the number of layers has little effect on the peak strength and cohesion, which is mainly related to the saturation of the hydrates in the model.

(2) Fine-grained mineral layers without hydrates play a major role in controlling the deformation modulus of HBS. When the coarse and fine grains are interlayered and hydrates occur in the coarse-grained layers, there is a good linear positive correlation between deformation modulus and layer number.

(3) When coarse and fine grains correspond to different mineral constituents, the material heterogeneity can further decrease the macroscopic mechanical parameters of HBS, such as peak strength, deformation modulus, and cohesion, which indicate that the mechanical strength will be overestimated if the homogeneous model is used for reservoir evaluation.

(4) The layering of sediment particles and hydrates results in anisotropy of the reservoir. The deformation modulus increases with an increase in the bedding dip angle, and the peak strength first decreases and then increases, with a minimum occurring at an angle of 60°. The anisotropic effect of sediment formation cannot be ignored, when evaluating reservoir strength in the region with complex structural conditions.

The research results have revealed the influence of the layered distribution characteristics of hydrates on the mechanical properties of HBS, which can provide the corresponding technical guidance for the engineering practice. However, the current work lacks experimental verification. In future work, it is proposed to carry out laboratory experiments on the HBS from Shenhu Sea area to test the developed research methodology.

Author Contributions: Conceptualization, Methodology, Writing—review and editing, Z.H.; Conceptualization, Methodology, Supervision, Resources, Funding acquisition, L.Z.; Writing—review and editing, J.Z.; Review and editing, Formal analysis, Z.P.; Formal analysis, S.W.; Formal analysis, R.L. All authors have read and agreed to the published version of the manuscript.

Funding: This research was funded by National Natural Science Foundation of China, grant number 42107190, 41972287 and 42277144.

Data Availability Statement: The data used to support the findings of this study are available from the corresponding author upon request.

Conflicts of Interest: The authors declare no conflict of interest.

References

1. Chong, Z.R.; Yang, S.H.B.; Babu, P.; Linga, P.; Li, X.S. Review of natural gas hydrates as an energy resource: Prospects and challenges. *Appl. Energy* **2016**, *162*, 1633–1652. [CrossRef]

2. Dong, H.; Wang, J.; Xie, Z.; Wang, B.; Zhang, L.; Shi, Q. Potential applications based on the formation and dissociation of gas hydrates. *Renew. Sustain. Energy Rev.* **2021**, *143*, 110928. [CrossRef]
3. Han, Z.; Zhang, L.; Zhou, J.; Pan, Z.; Wang, S.; Li, R. Effects of Hydrate Occurring Mechanisms and Saturation on the Mechanical Properties of Hydrate-bearing Sediments: Numerical Study based on Simplified DEM simulation. *J. Nat. Gas Sci. Eng.* **2022**, *108*, 104804. [CrossRef]
4. Dong, H.; Zhang, L.; Wang, J. Formation, Exploration, and Development of Natural Gas Hydrates. *Energies* **2022**, *15*, 5951. [CrossRef]
5. Bosikov, I.I.; Klyuev, R.V.; Silaev, I.V.; Pilieva, D.E. Estimation of multistage hydraulic fracturing parameters using 4D simulation. *Min. Sci. Technol.* **2023**, *8*, 141–149. [CrossRef]
6. Brown, N.M.; Brown, M. Tracer dispersion due to non-Newtonian fluid flows in hydraulic fractures with different geometries and porous walls. *J. Hydrol.* **2023**, *622*, 129644. [CrossRef]
7. Manjunath, G.L.; Liu, Z.; Jha, B. Multi-stage hydraulic fracture monitoring at the lab scale. *Eng. Fract. Mech.* **2023**, *289*, 109448. [CrossRef]
8. Locat, J.; Lee, H.J. Submarine landslides: Advances and challenges. *Can. Geotech. J.* **2002**, *39*, 193–212. [CrossRef]
9. Sultan, N.; Cochonat, P.; Foucher, J.R. Effect of gas hydrates melting on seafloor slope instability. *Mar. Geol.* **2004**, *213*, 379–401. [CrossRef]
10. Uchida, S.; Lin, J.-S.; Myshakin, E.M.; Seol, Y.; Boswell, R. Numerical simulations of sand migration during gas production in hydrate-bearing sands interbedded with thin mud layers at site NGHP-02-16. *Mar. Pet. Geol.* **2018**, *108*, 639–647. [CrossRef]
11. Lijith, K.P.; Malagar, B.R.C.; Singh, D.N. A comprehensive review on the geomechanical properties of gas hydrate bearing sediments. *Mar. Pet. Geol.* **2019**, *104*, 270–285. [CrossRef]
12. Bazaluk, O.; Sai, K.; Lozynskyi, V.; Petlovanyi, M.; Saik, P. Research into Dissociation Zones of Gas Hydrate Deposits with a Heterogeneous Structure in the Black Sea. *Energies* **2021**, *14*, 1345. [CrossRef]
13. Rutqvist, J.; Moridis, G.; Grover, T.; Silpngarmlert, S.; Collett, T.; Holdich, S. Coupled multiphase fluid flow and wellbore stability analysis associated with gas production from oceanic hydrate-bearing sediments. *J. Pet. Sci. Eng.* **2012**, *92–93*, 65–81. [CrossRef]
14. Fujii, T.; Suzuki, K.; Takayama, T.; Tamaki, M.; Komatsu, Y.; Konno, Y.; Yoneda, J.; Yamamoto, K.; Nagao, J. Geological setting and characterization of a methane hydrate reservoir distributed at the first offshore production test site on the Daini-Atsumi Knoll in the eastern Nankai Trough, Japan. *Mar. Pet. Geol.* **2015**, *66*, 310–322. [CrossRef]
15. Ye, J.-L.; Qin, X.-W.; Xie, W.-W.; Lu, H.-L.; Ma, B.-J.; Qiu, H.-J.; Liang, J.-Q.; Lu, J.-A.; Kuang, Z.-G.; Cheng, F.; et al. The second natural gas hydrate production test in the South China Sea. *China Geol.* **2020**, *3*, 197–209. [CrossRef]
16. Ye, J.-L.; Qin, X.-W.; Xie, W.-W.; Lu, H.-L.; Ma, B.-J.; Qiu, H.-J.; Liang, J.-Q.; Lu, J.-A.; Kuang, Z.-G. Characterization of gas hydrate reservoirs by integration of core and log data in the Ulleung Basin, East Sea. *Mar. Pet. Geol.* **2013**, *47*, 30–42. [CrossRef]
17. Torres, M.; Tréhu, A.; Cespedes, N.; Kastner, M.; Wortmann, U.; Kim, J.-H.; Long, P.; Malinverno, A.; Pohlman, J.; Riedel, M.; et al. Methane hydrate formation in turbidite sediments of northern Cascadia, IODP Expedition 311. *Earth Planet. Sci. Lett.* **2008**, *271*, 170–180. [CrossRef]
18. Zhang, H.; Lu, H.L.; Liang, J.Q. The methane hydrate accumulation controlled compellingly by sediment grain at Shenhu, northern South China Sea. *Chin. Sci. Bull.* **2016**, *61*, 388–397. (In Chinese) [CrossRef]
19. Yoneda, J.; Oshima, M.; Kida, M.; Kato, A.; Konno, Y.; Jin, Y.; Jang, J.; Waite, W.F.; Kumar, P.; Tenma, N. Pressure core based onshore laboratory analysis on mechanical properties of hydrate-bearing sediments recovered during India's National Gas Hydrate Program Expedition (NGHP) 02. *Mar. Pet. Geol.* **2018**, *108*, 482–501. [CrossRef]
20. Pecher, I.A.; Holbrook, W.S.; Sen, M.K.; Lizarralde, D.; Wood, W.T.; Hutchinson, D.R.; Dillon, W.P.; Hoskins, H.; Stephen, R.A. Seismic anisotropy in gas-hydrate- and gas-bearing sediments on the Blake Ridge, from a walkaway vertical seismic profile. *Geophys. Res. Lett.* **2003**, *30*, 291–305. [CrossRef]
21. Liu, J.-W.; Li, X.-S.; Kou, X.; Wang, Y.; Li, L.-J. Analysis of Hydrate Heterogeneous Distribution Effects on Mechanical Characteristics of Hydrate-Bearing Sediments. *Energy Fuel* **2021**, *35*, 4914–4924. [CrossRef]
22. Uchida, S.; Soga, K.; Yamamoto, K. Critical state soil constitutive model for methane hydrate soil. *J. Geophys. Res. Solid Earth* **2012**, *117*, B03209. [CrossRef]
23. Hyodo, M.; Li, Y.; Yoneda, J.; Nakata, Y.; Yoshimoto, N.; Nishimura, A.; Song, Y. Mechanical behavior of gas-saturated methane hydrate-bearing sediments. *J. Geophys. Res. Solid Earth* **2013**, *118*, 5185–5194. [CrossRef]
24. Miyazaki, K.; Tenma, N.; Sakamoto, Y.; Yamaguchi, T.; Okubo, S. Effects of Methane Hydrate Saturation and Confining Pressure on Strain-Rate Dependence of Artificial Methane-Hydrate-Bearing Sediment in Triaxial Compression Test. *Int. J. Offshore Polar* **2012**, *22*, 90–96. [CrossRef]
25. Choi, J.H.; Dai, S.; Lin, J.S.; Seol, Y. Multistage Triaxial Tests on Laboratory-Formed Methane Hydrate-Bearing Sediments. *J. Geophys. Res. Solid Earth* **2018**, *123*, 3347–3357. [CrossRef]
26. Priest, J.A.; Hayley, J.L. Strength of laboratory synthesized hydrate-bearing sands and their relationship to natural hydrate-bearing sediments. *J. Geophys. Res. Solid Earth* **2019**, *124*, 12556–12575. [CrossRef]
27. Zhou, M.; Soga, K.; Yamamoto, K. Upscaled Anisotropic Methane Hydrate Critical State Model for Turbidite Hydrate-Bearing Sediments at East Nankai Trough. *J. Geophys. Res. Solid Earth* **2018**, *123*, 6277–6298. [CrossRef]
28. Li, Y.L.; Wu, Q.; Wu, P.; Liu, W.G. Mechanical Properties of Methane Hydrate Interbedded with Clayey Sediments. *J. Energy Nat. Res.* **2018**, *7*, 24–31. [CrossRef]

29. Li, Y.; Dong, L.; Wu, N.; Nouri, A.; Liao, H.; Chen, Q.; Sun, J.; Liu, C. Influences of hydrate layered distribution patterns on triaxial shearing characteristics of hydrate-bearing sediments. *Eng. Geol.* **2021**, *294*, 106375. [CrossRef]
30. Waite, W.F.; Santamarina, J.C.; Cortes, D.D.; Dugan, B.; Espinoza, D.N.; Germaine, J.; Jang, J.; Jung, J.W.; Kneafsey, T.J.; Shin, H.; et al. Physical properties of hydrate-bearing sediments. *Rev. Geophys.* **2009**, *47*, 465–484. [CrossRef]
31. Masui, A.; Haneda, H.; Ogata, Y.; Aoki, K. Effects of methane hydrate formation on shear strength of synthetic methane hydrate sediments. In Proceedings of the Fifteenth International Offshore and Polar Engineering Conference, Seoul, Republic of Korea, 19–24 June 2005; International Society of Offshore and Polar Engineers: Seoul, Republic of Korea, 2005.
32. Winters, W.; Waite, W.; Mason, D.; Gilbert, L.; Pecher, I. Methane gas hydrate effect on sediment acoustic and strength properties. *J. Pet. Sci. Eng.* **2007**, *56*, 127–135. [CrossRef]
33. Miyazaki, K. Triaxial compressive properties of artificial methane-hydrate-bearing sediment. *J. Geophys. Res. Solid Earth* **2011**, *116*, B06102. [CrossRef]
34. Hyodo, M.; Wu, Y.; Nakashima, K.; Kajiyama, S.; Nakata, Y. Influence of Fines Content on the Mechanical Behavior of Methane Hydrate-Bearing Sediments. *J. Geophys. Res. Solid Earth* **2017**, *122*, 7511–7524. [CrossRef]
35. Kajiyama, S.; Wu, Y.; Hyodo, M.; Nakata, Y.; Nakashima, K.; Yoshimoto, N. Experimental investigation on the mechanical properties of methane hydrate-bearing sand formed with rounded particles. *J. Nat. Gas. Sci. Eng.* **2017**, *45*, 96–107. [CrossRef]
36. Shen, S.; Sun, X.; Wang, L.; Song, Y.C.; Li, Y.H. Effect of Temperature on the Mechanical Properties of Hydrate-Bearing Sand under Different Confining Pressures. *Energy Fuel* **2021**, *35*, 4106–4117. [CrossRef]
37. Liu, W.; Pan, D.; Shen, S.; You, Z.; Zhao, Y.; Sun, X. Experimental Study on Mechanical Properties of Hydrate-Bearing Sand: The Influence of Sand-Water Mixing Methods. *Energies* **2021**, *14*, 2554. [CrossRef]
38. Ginsburg, G.; Soloviev, V.; Matveeva, T.; Andreeva, T. Sediment Grain-Size Control on Gas Hydrate Presence, Sites 994, 995, and 997, Scientific Results, Proc. Ocean Drill. *Program Sci. Results* **2000**, *164*, 237–245. [CrossRef]
39. Uchida, T.; Takeya, S.; Chuvilin, E.M.; Ohmura, R.; Nagao, J.; Yakushev, V.S.; Istomin, V.A.; Minagawa, H.; Ebinuma, T.; Narita, H. Decomposition of methane hydrates in sand, sandstone, clays, and glass beads. *J. Geophys. Res. Atmos.* **2004**, *109*, B05206. [CrossRef]
40. Tréhu, A.; Long, P.; Torres, M.; Bohrmann, G.; Rack, F.; Collett, T.; Goldberg, D.; Milkov, A.; Riedel, M.; Schultheiss, P.; et al. Three-dimensional distribution of gas hydrate beneath southern hydrate ridge: Constraints from ODP leg 204. *Earth Planet. Sci. Lett.* **2004**, *222*, 845–862. [CrossRef]
41. Qin, X.-W.; Lu, J.-A.; Lu, H.-L.; Qiu, H.-J.; Liang, J.-Q.; Kang, D.-J.; Zhan, L.-S.; Lu, H.-F.; Kuang, Z.-G. Coexistence of natural gas hydrate, free gas and water in the gas hydrate system in the Shenhu Area, South China Sea. *China Geol.* **2020**, *3*, 210–220. [CrossRef]
42. Sun, S.-C.; Liu, C.-L.; Ye, Y.-G.; Liu, Y.-F. Phase behavior of methane hydrate in silica sand. *J. Chem. Thermodyn.* **2014**, *69*, 118–124. [CrossRef]
43. Potyondy, D.O.; Cundall, P.A. A Bonded-Particle Model for Rock. *Int. J. Rock Mech. Min.* **2004**, *41*, 1329–1364. [CrossRef]
44. Han, Z.; Zhou, J.; Zhang, L. Influence of Grain Size Heterogeneity and In-Situ Stress on the Hydraulic Fracturing Process by PFC2D Modeling. *Energies* **2018**, *11*, 1413. [CrossRef]
45. Liu, C.; Ye, Y.; Meng, Q.; He, X.; Lu, H.; Zhang, J.; Liu, J.; Yang, S. The characteristics of gas hydrates recovered from Shenhu area in the South China Sea. *Mar. Geol.* **2012**, *307–310*, 22–27. [CrossRef]
46. Wang, L.; Li, Y.; Shen, S.; Liu, T.; Zhao, J. Untrained triaxial tests on water-saturated methane hydrate-bearing clayey-silty sediments of the South China Sea. Can. *Geotech. J.* **2020**, *58*, 351–366. [CrossRef]
47. Han, Z.; Zhang, L.; Azzam, R.; Zhou, J.; Wang, S. A statistical index indicating the degree and mechanical effects of grain size heterogeneity in rocks. *Eng. Geol.* **2021**, *293*, 106292. [CrossRef]
48. Wang, L.; Li, Y.; Shen, S.; Liu, W.; Sun, X.; Liu, Y.; Zhao, J. Mechanical Behaviors of Gas Hydrate-bearing Clayey Sediments of the South China Sea. *J. Environ. Geotech.* **2019**, *9*, 210–222. [CrossRef]
49. Miyazaki, K.; Tenma, N.; Aoki, K.; Yamaguchi, T. A Nonlinear Elastic Model for Triaxial Compressive Properties of Artificial Methane-Hydrate-Bearing Sediment Samples. *Energies* **2012**, *5*, 4057–4075. [CrossRef]
50. Liu, J.; Zhao, Y.; Sang, S.; Zeng, Z.; Hua, L.; Kong, L. Triaxial Tests of Hydrate-Bearing Clayey-Silty Sediments Under Different Hydrate Saturations and Effective Confining Pressures. *Energy Fuel* **2022**, *36*, 14042–14054. [CrossRef]

Disclaimer/Publisher's Note: The statements, opinions and data contained in all publications are solely those of the individual author(s) and contributor(s) and not of MDPI and/or the editor(s). MDPI and/or the editor(s) disclaim responsibility for any injury to people or property resulting from any ideas, methods, instructions or products referred to in the content.